HOT MEDIUM

Gas with $T >$ few$\times 10^5$ K to $T \lesssim 10^7$ K, at low density (in approximate P equilibrium).

Created by shock → winds
→ SNe

The HIM fills interiors of SNRs, as well as the supershells produced by the combined winds/SN from massive stars.

$M_* > 50\, M_\odot$, $v_{wind} \sim 2000$ km/s, $\dot{M} \sim 10^{-6}\, M_\odot\, yr^{-1}$

over $t \sim$ few$\times 10^6$ yr $\Rightarrow E^{TOT}_{kin} \sim 10^{51}$ erg

1 SN → $E_k - 10^{51}$ erg

Type I SN → isolated, low mass stars ⇒ energy dispersed

Type II → high mass, clustered ⇒ energy concentrated
most common

Phases: non radiative, radiative, snow-plow

Local SB: Eridanus (500pc)
from previous generations in Orion
250 pc size, emits 0.75 keV photons (~~X~~-rays)
hot = young
1 kpc region emits softer ~~X~~-rays, 0.25 keV

North polar spur
Scorpius-Ophiuchus assoc.

Local bubble → contains the sun (Snowden)

SB may be powerful enough to break ~~through~~ through colder ISM in the galactic disk → "chimneys" → covering factor is uncertain, but estimated 10-20%.

10^6 K in center of bubbles
10^5 K in walls

Diagnostics

HIM $\begin{cases} \text{soft-x rays} \\ \text{UV absorption and emission lines} \end{cases}$

Soft x-rays → $T \gtrsim 0.7 \times 10^6$ K

(Snowden et al. 1995, 1997; ROSAT Maps)

Opacity of ISM limits distance: $N_{HI,max}(0.25\,keV) = 0.6 \times 10^{20}\,cm^{-2}$

$N_{HI,max}(0.75\,keV) = 20 \times 10^{20}$

~700 pc @ 1 cm^{-3}

Emission dominate by resonant lines of heavy elements for $T \lesssim 30 \times 10^6$ K ⇒ need detailed theoretical spectrum in order to determine gas temperature

In general, $I_{band} \propto \int n_e^2 \cdot \mathcal{E}(T)_{band} \cdot e^{-\tau_{band}}\, dz$

collisionally excited

⇒ band ratios measure $\langle n_e^2 \rangle$ and T → $T \sim 10^6$ K

Typical $n \sim 0.003\ cm^{-3}$

For colder gas: UV

Line	T_{max} (K)
Si IV	0.6×10^5
C IV	1.0
S VI	2.0
N V	1.8
O VI	3.0
Fe X	12
Fe XIV	20

→ Temp for ion's max. abundance

Since ionization and recombination are collisional, both are $\propto n_e \cdot n_I \cdot f(T) \Rightarrow$ ionization fraction is indep. of n!

$\Rightarrow$ if a species is observed, $T > T_{max}$ for previous ion down

(C IV obs $\Rightarrow T > T_{C\,III\,max}$)

Absorption studies:

absorption strength $\propto \int n\,dz$

emission may also be present, $\propto \int n^2 dz$

$\Rightarrow$ Together we obtain n, and T from T_{max} for ion

EUVE, COPERNICUS

$P/k \sim 2000-4000 \text{ cm}^{-3}\text{K}$, $T \sim 1-3\times10^5$

Jenkins 1978

Dixon, Davidson, Ferguson 1996

Martin & Bowyer 1990

Hot gas with scale height ~ 3 kpc

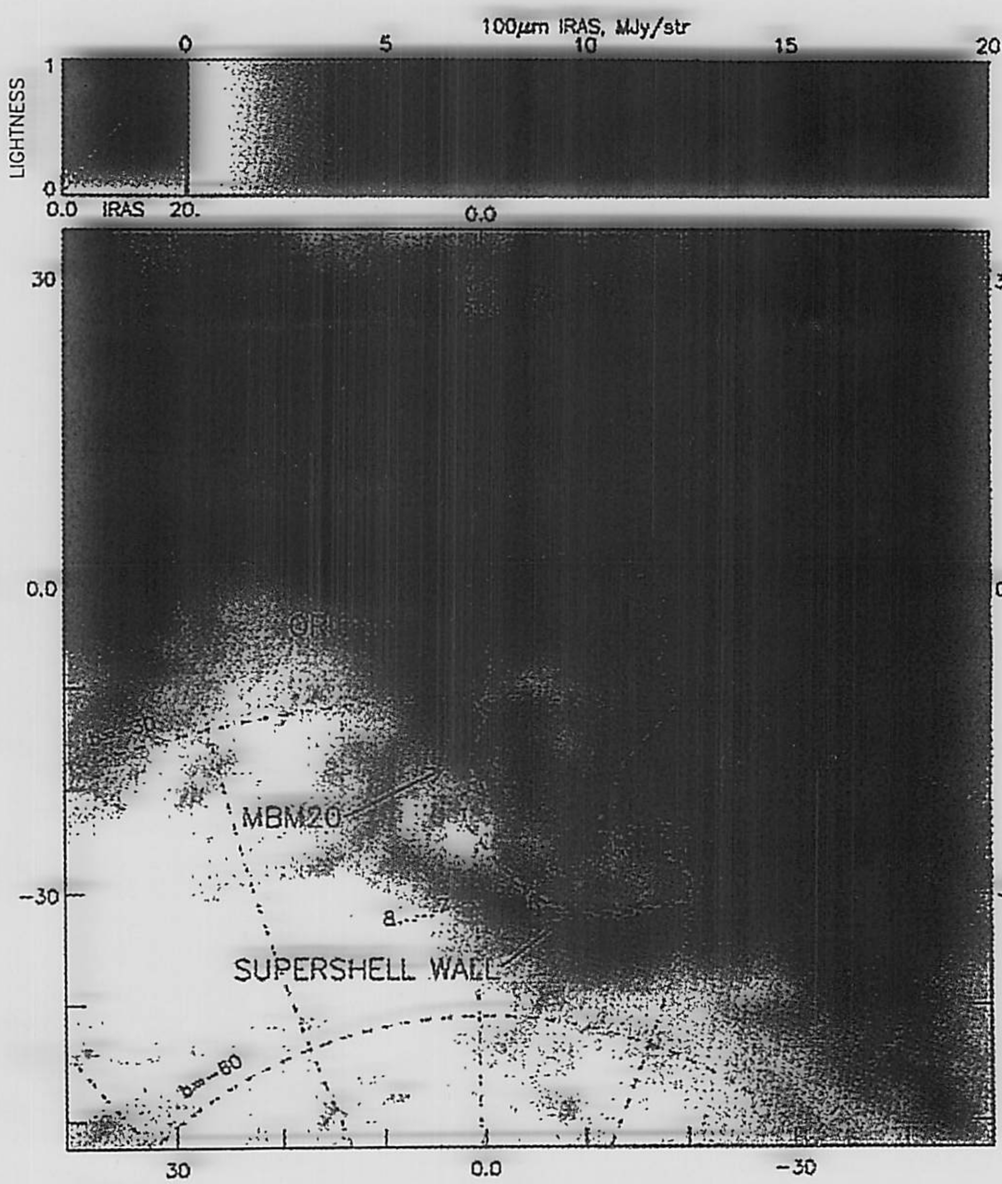

Figure 3. 100 μm emission from IRAS. To obtain $N(HI)_{20}$ in regions of low column density, multiply by about 1.5. See caption for Figure 1.

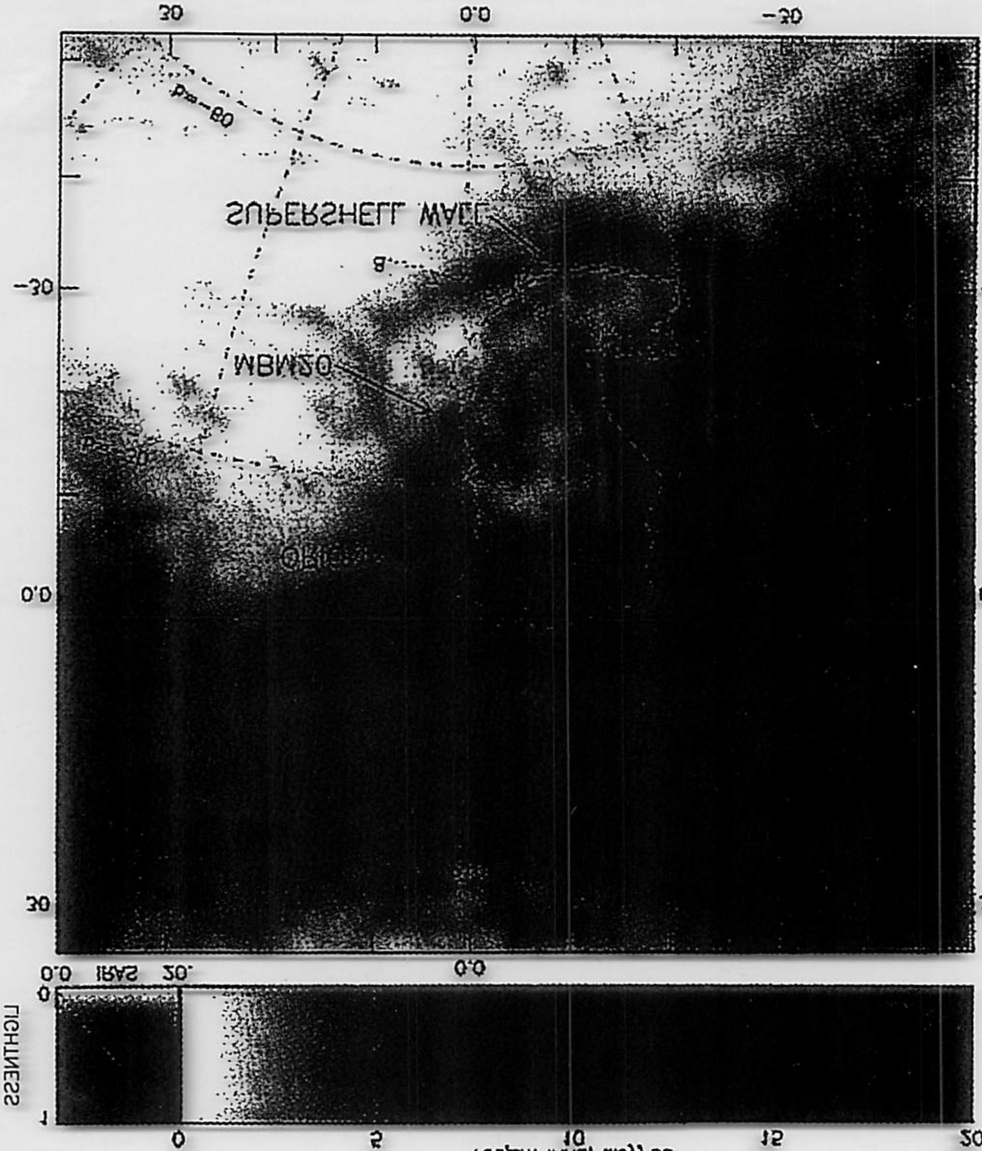

Figure 3. 100 μm emission from IRAS. To obtain $N(HI)_{20}$ in regions of low column density, multiply by about 1.5. See caption for Figure 1.

3/4 keV RASS - Snowden et al (1995, 1997)

T ~ 2x10^6 K Hot gas

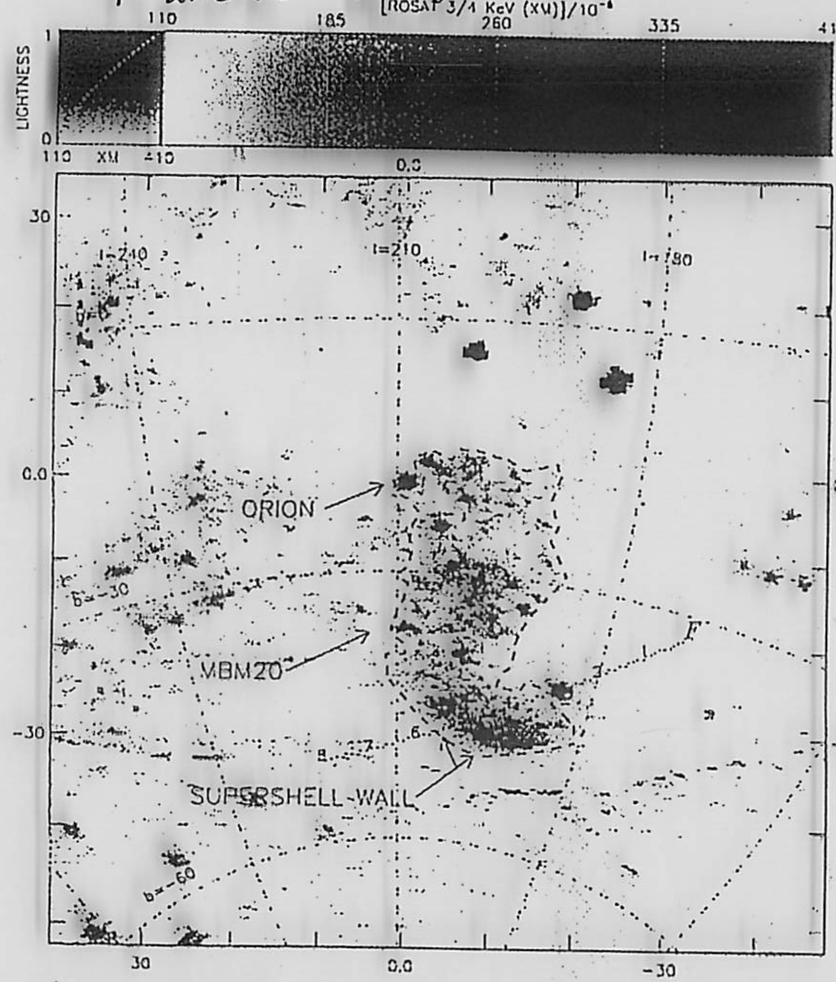

Figure 1. XM-band emission ($\frac{3}{4}$ keV, from gas at $T \sim 2\times10^6$ K) from Snowden et al (1995b). The grey scale is calibrated by the colorbar on top right in units of 10^{-6} ROSAT counts s^{-1} $arcmin^{-2}$; the small square plot on top left shows the same calibration with a graph. Saturated parts of the image exceed the colorbar maximum. Galactic coordinates are labelled on the dashed grid lines. Numbers outside the border refer to angular distance (degrees) from the center of the projection (which is not the center of the image). The heavy dashed line outlines the sharp boundary of the XM emission and the dotted line defines a "slit" for the position-velocity diagrams.

Eridanus Superbubble

1/4 keV RASS

T ~ 1x10^6 keV

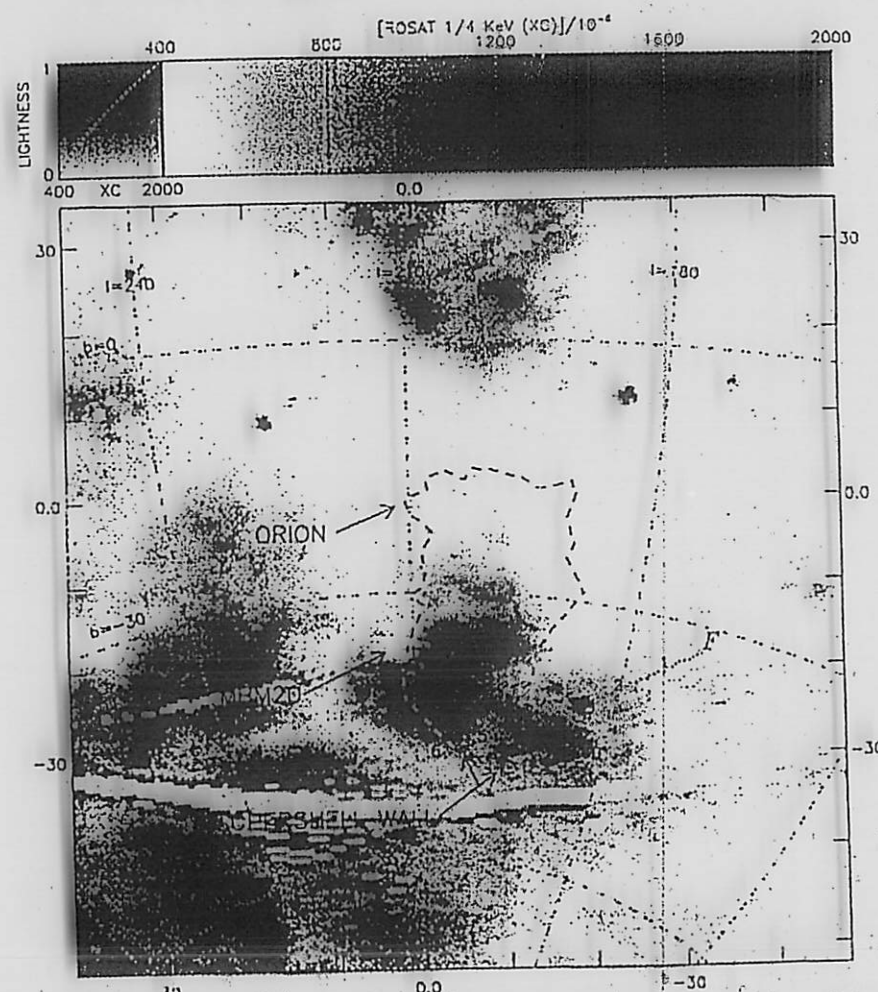

Figure 2. XC-band emission ($\frac{1}{4}$ keV, from gas at $T \sim 1 \times 10^6$ K) from Snowden et al (1995b). See caption for Figure 1.

3/4 keV RASS - Snowden et al (1995, 1997)

T ~ 2x10^6 K Hot gas

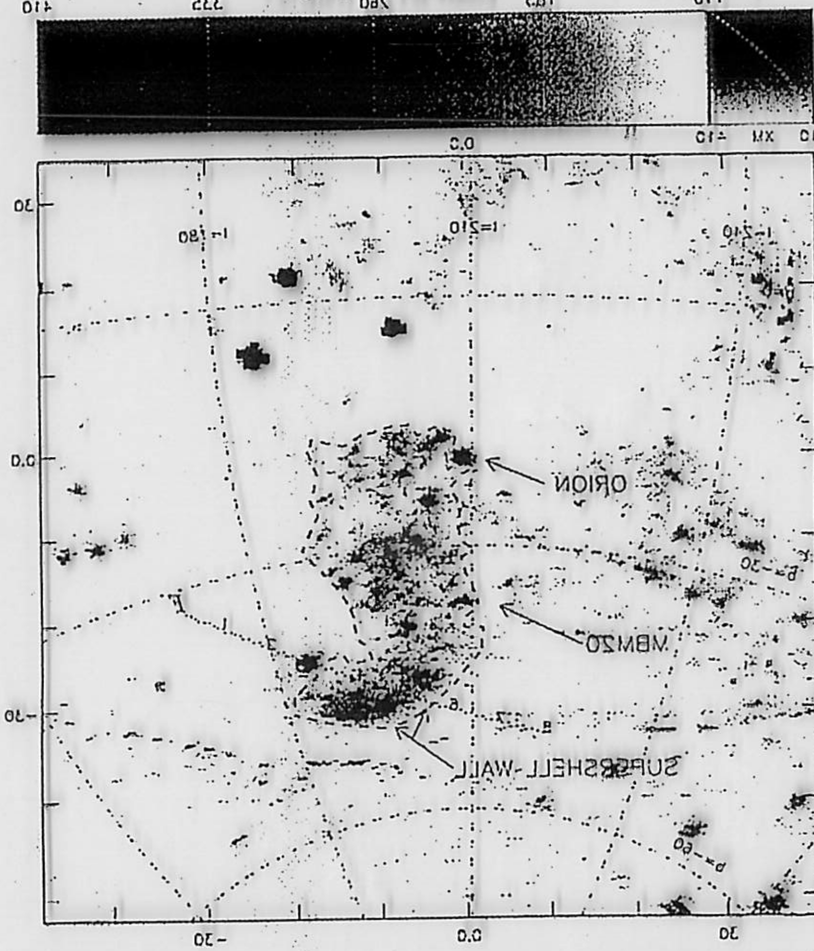

Figure 1. XM-band emission ($\frac{3}{4}$ keV, from gas at $T \sim 2 \times 10^6$ K) from Snowden et al (1995b). The grey scale is calibrated by the colorbar on top right in units of 10^{-6} ROSAT counts s^{-1} arcmin^{-2}; the small square plot on top left shows the same calibration with a graph. Saturated parts of the image exceed the colorbar maximum. Galactic coordinates are labelled on the dashed grid lines. Numbers outside the border refer to angular distance (degrees) from the center of the projection (which is not the center of the image). The heavy dashed line outlines the sharp boundary of the XM emission and the dotted line defines a "slit" for the position-velocity diagrams.

Eridanus Superbubble

1/4 keV RASS

T ~ 1x10^6 keV

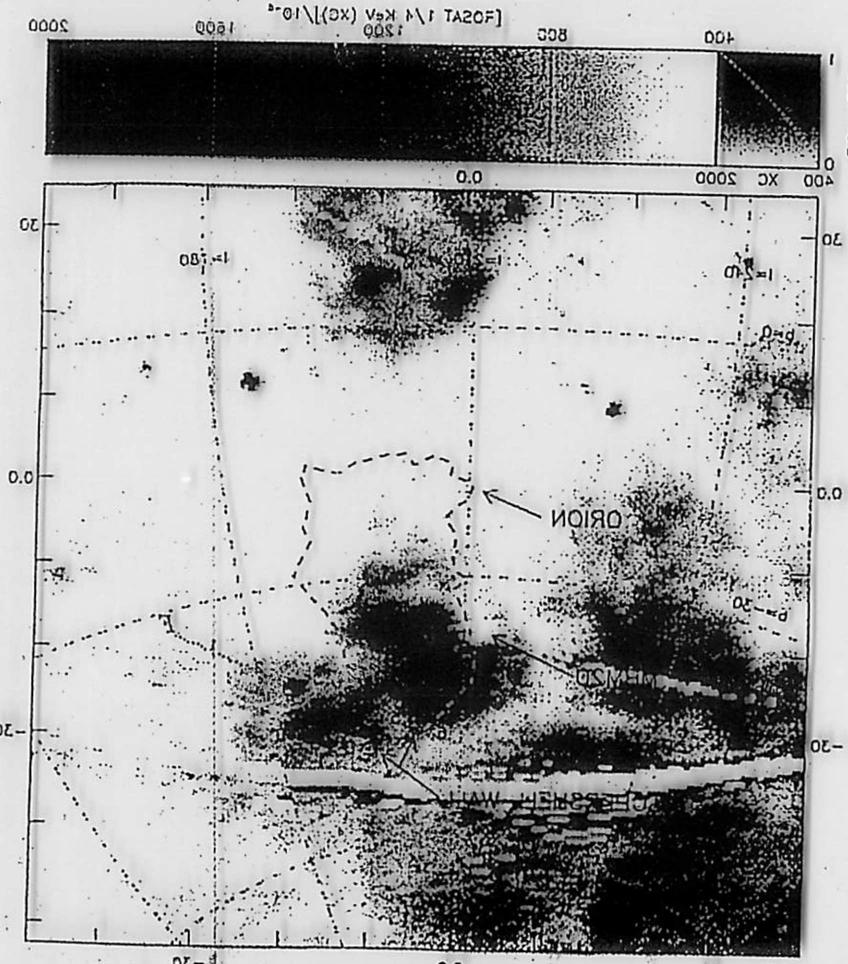

Figure 2. XC-band emission ($\frac{1}{4}$ keV, from gas at $T \sim 1 \times 10^6$ K) from Snowden et al (1995b). See caption for Figure 1.

The Local ISM (500 pc)

- **Sun** is at the center
  - Brightest stars (giants & supergiants)
  - Denser portions of the ISM (orange)

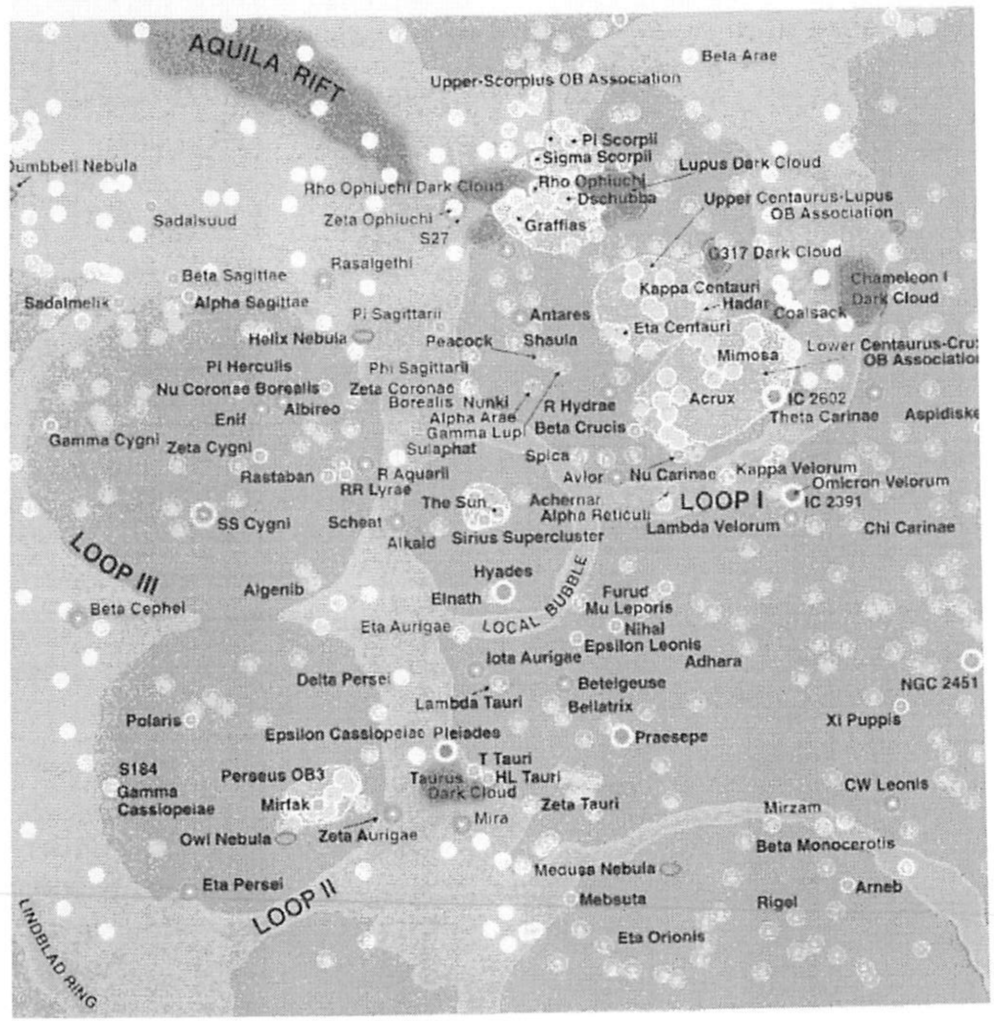

The Local ISM (120 pc)

- **Sun** is at the center, Galactic Center at top
  - –OB stars (blue), AFG (yellow), and ; KM (orange)
  - –Rings of denser gas (yellow)
    - 3-d shells of "warm"gas (~5000 K), containing low-density, hot gas (~$10^{5\text{-}6}$ K)
    - Supernovae & winds from stars in OB associations
- Interior of the Local Bubble
  - –n ~ 0.05 - 0.07 cm^{-3}
- Local Bubble is not spherical
  - –The long axis ⊥ to the Galactic plane
  - –Density gradients or colliding SNR
- Above Arcturus is the "Wall" of denser gas
  - –Like Loop 1, the wall appears to be driven by the Sco-Cen association
- *Local Fluff* is a denser region (~ 0.1 cm^{-3}) recently encountered by the Sun
  - –The Sun is headed to the left at ~ 20 km/s plowing through the Local Fluff

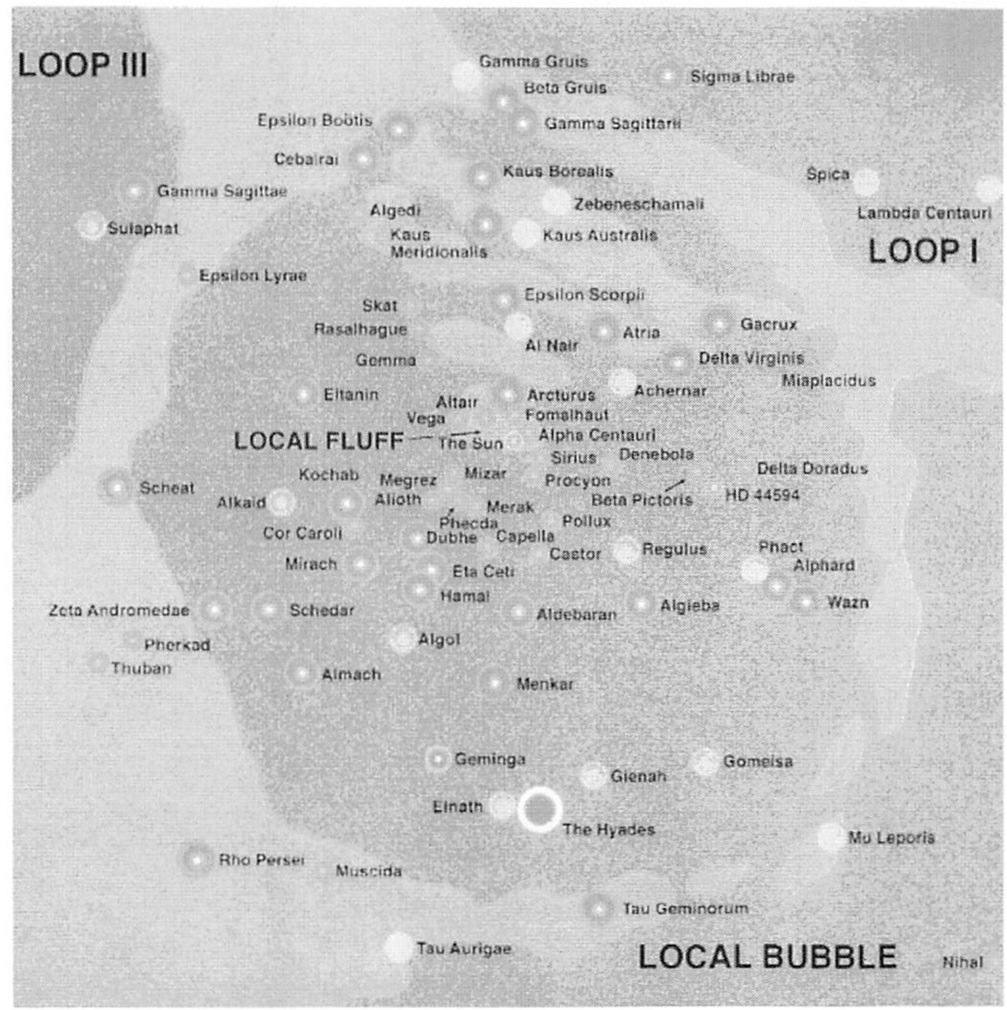

From The limited # of line components (~ 6/kpc, Jenkins 78)
$T \sim 10^5$ K gas seems to be in discreet structures (walls)
Lines are not broad $\Rightarrow$ not in expanding shell
This is expected to arise in conductive interface regions
(would need $V_{shock} \sim 150$ km/s to produce $T \sim 3\times10^5$ K,
but line widths are $V_{FWHM} \lesssim 30$ km/s)

Cooling

For very high temperatures nuclei are stripped of e^-, so cooling is from Thermal Bremsstrahlung ($T > 3\times10^7$ K)

charge of ion

$$\varepsilon_\nu^{ff} = \rho j_\nu = \sum_i n(z_i)\, n_e \left(\frac{2 m_e}{3\pi kT}\right)^{1/2} \left[\frac{32\pi^2 Z_i^2 e^6}{3 m_e^2 c^3}\right] \bar{g}_{ff}(\nu) \cdot e^{-h\nu/kT}$$ (Shu 15.28)

$$= 6.8\times10^{-38} Z^2 n_e n_i T^{-1/2} e^{-h\nu/kT} \bar{g}_{ff}(\nu)$$ (R-L 5.14b)

For $h\nu \ll kT$ (hot gas)

$$g = \begin{cases} \frac{\sqrt{3}}{2\pi}\left[\ln\left(\frac{8k^3T^3}{\pi^2 e^4 m_e \nu^2 Z^2}\right) - 5\gamma\right] & \text{radio} \\ \frac{\sqrt{3}}{\pi}\ln\left(\frac{kT}{h\nu}\right) & \text{X-ray} \\ \sim 1 & \text{optical} \end{cases}$$

$\gamma = 0.577$ Euler's constant

radio: Shu HW 4 prob 3, Osterbrock eq. 4.30

X-ray: Longhair eq. 3.17

Total emissivity at all ν is

$$\varepsilon = \int \rho j_\nu d\nu = 1.4\times10^{-27} T^{1/2} n_e n_i Z^2 \bar{g}_B$$ (R-L 5.15b)

$\bar{g}_B = 1.1 - 1.5$

For solar abundances, including contrib. from high Z,

$$\Lambda_{ff} = 2.3 \times 10^{-24} T_6^{1/2} n^2 \quad \text{erg cm}^{-3}\,\text{s}^{-1}$$

For lower T → line emission from collisional excitat
in metals

From integration and fitting:

$$\Lambda_{lines} \cong 1.6 \times 10^{-22} T_6^{-0.6} n^2 \; \text{erg cm}^{-3}\,\text{s}^{-1} \quad (\text{To} \sim 2\times \text{fa}$$

$$1.1 \times 10^{-22} T_6^{-0.7} n^2 \text{ (Draine's Book)}$$

(Raymond, Cox, Smith 1976
ApJ 204, 290)

Cooling Times:

$$t_{cool} \approx \frac{3kTm_H}{\mathcal{E}} \sim \begin{cases} \dfrac{3kT^{1/2}}{2.4\times 10^{-27} n} & \text{Brems } (T \gtrsim 1 \\ \dfrac{3kT^{1.6}}{6.4\times 10^{-19} n_H} & \text{lines} \end{cases}$$

$$\text{For } T \sim 10^6\,\text{K}, \quad n \sim 0.001\,\text{cm}^{-3} \quad t_{cool} = \begin{cases} 1.7\times 10^{17}\,\text{s} \sim 6\times 1 & \text{Brems} \\ 2.6 \times 10^{15}\,\text{s} \sim 10 & \text{lines} \end{cases}$$

⇒ Cooling time for low density, high Temp. is very long if we only rely on local processes.

Note: cooling from inelastic collisions with grains could be important if grains survive the shock. But even if they do they would be slowly destro by sputtering.

$$t_{sput} \sim \frac{\overset{\text{size of grain}}{a}}{da/dt} \sim 10^6 \frac{a\,(\mu m)}{n_e}\ \text{yr} \qquad T > 10^6\,\text{K}$$

Draine & Salpeter (19

For dust cooling, the heating rate of dust grains immersed in ~~plasma~~ gas is

$$H(a,T,n) = \left(\frac{32}{\pi m}\right)^{1/2} \pi a^2 \, n(kT)^{3/2} \, h(a,T)$$

grain size — a; Temp. of gas — T; density — n; mass of ~~plasma~~ gas particles — m

Dwek (1987)

$h(a,T)$ is the effective grain "heating efficiency" given by Dwek & Werner (1981)

⇒ The cooling of a dusty plasma is:

$$\Lambda_d(T) = \frac{m_d}{n_e m_H} \int H(a,T,n) \cdot f(a) \, da$$

$f(a)$ — grain size distribution

show Fig 4 of Dwek 1987.

It can be dominant over $T = 10^6$ K, if dust survives.

However, hot gas may also cool by conduction. e carry heat away into the surroundings. Cool gas doesn't do this: radiation is much more efficient.

⇒ e need to carry energy, but the magnetic field structure limits their mobility.

Raymond, Cox, + Smith (1976) ApJ 204, 290

(Equilibrium-ionization) Cooling in Low-Density Hot Plasma

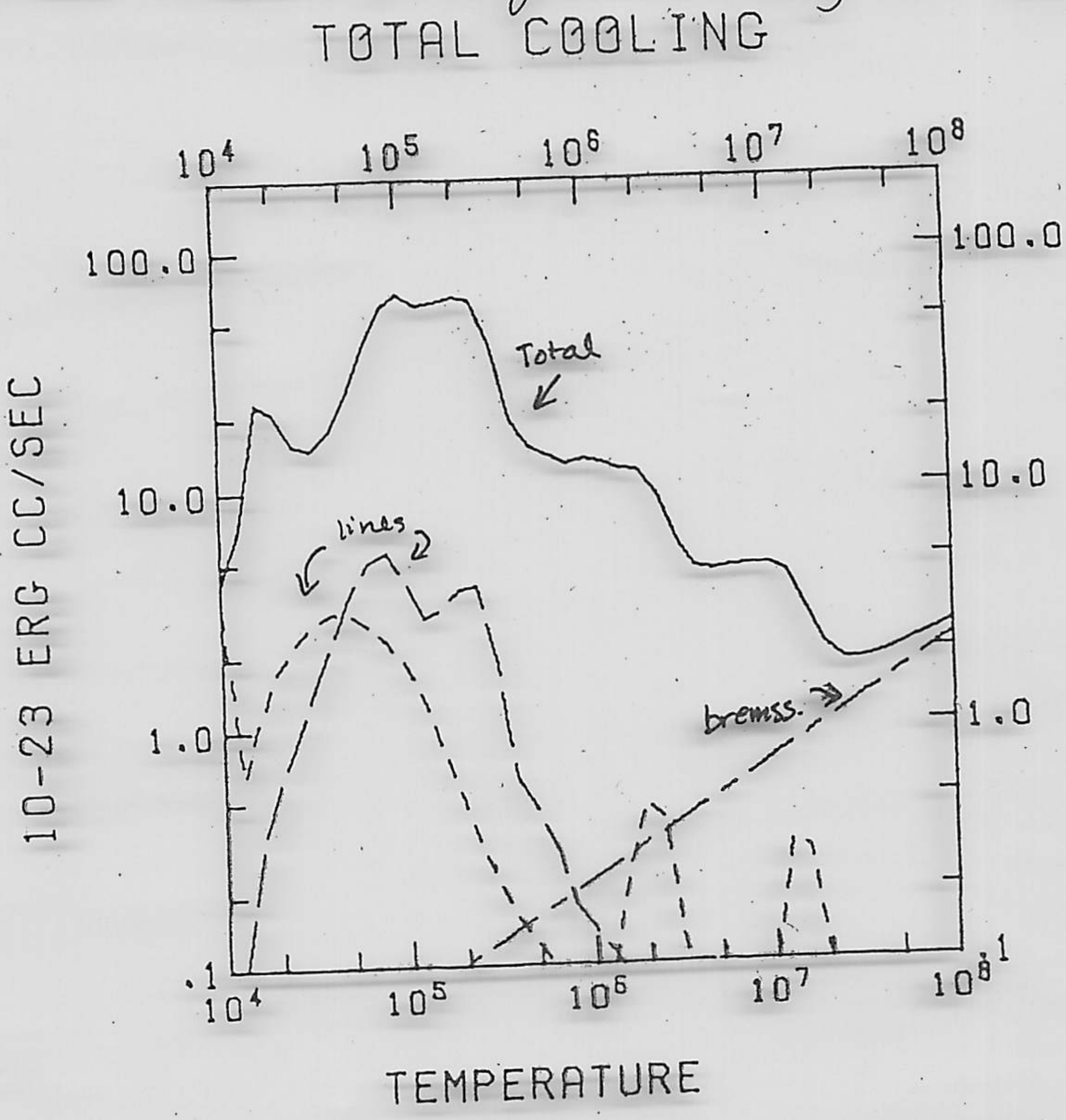

FIG. 1.—Total cooling coefficient (————), forbidden line cooling (- - - - - - - -), semiforbidden line cooling (— — — —), and bremsstrahlung (— - — - — -).

details in Raymond + Smith (1977) ApJS 35, 419

Raymond, Cox, + Smith (1976) ApJ 204, 290

(Equilibrium-ionization) Cooling in Low-Density Hot Plasma

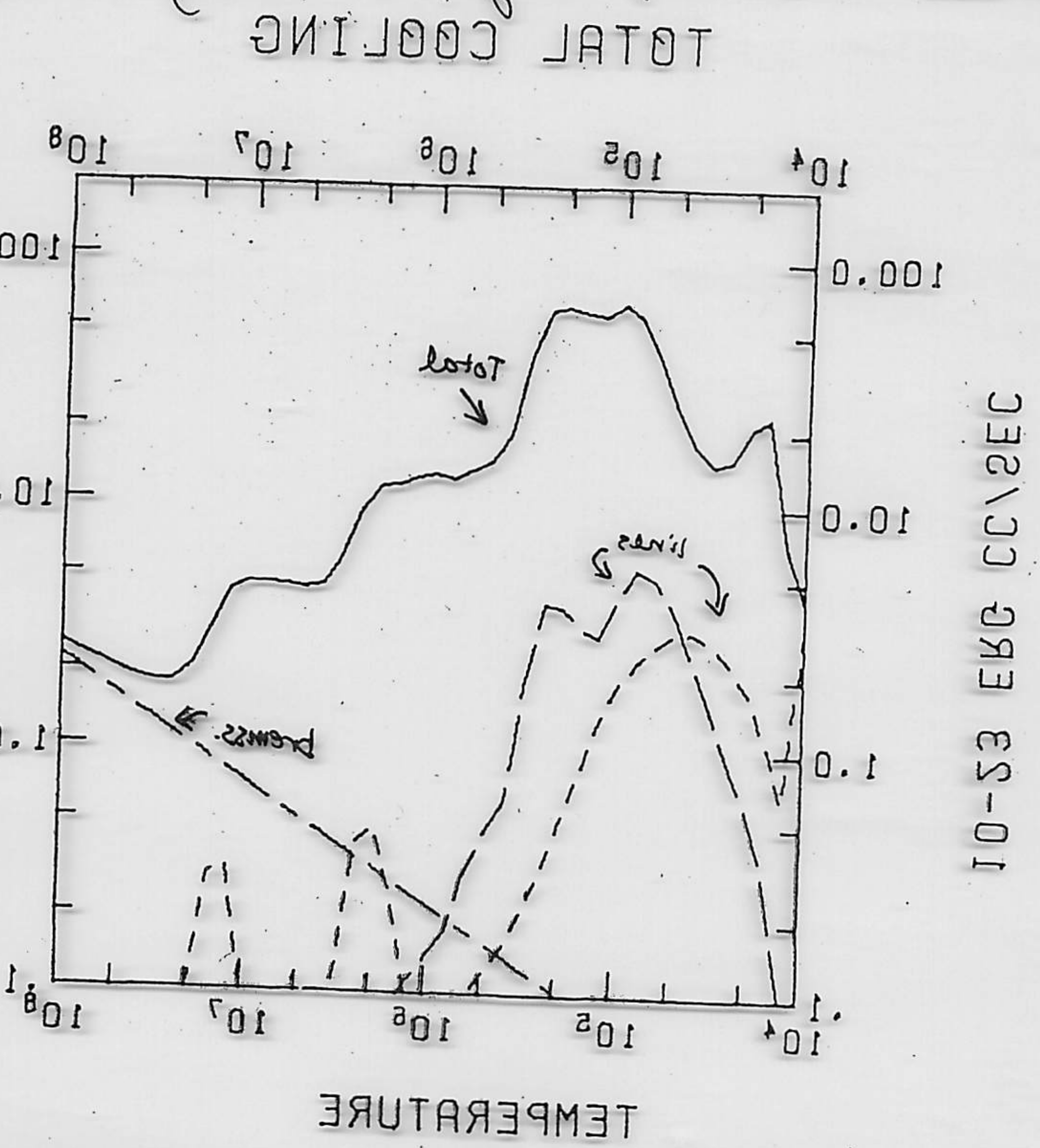

FIG. 1.—Total cooling coefficient (———), forbidden line cooling (-------), semiforbidden line cooling (— — —), and bremsstrahlung (— — — —).

details in Raymond + Smith (1977) ApJS 35, 419

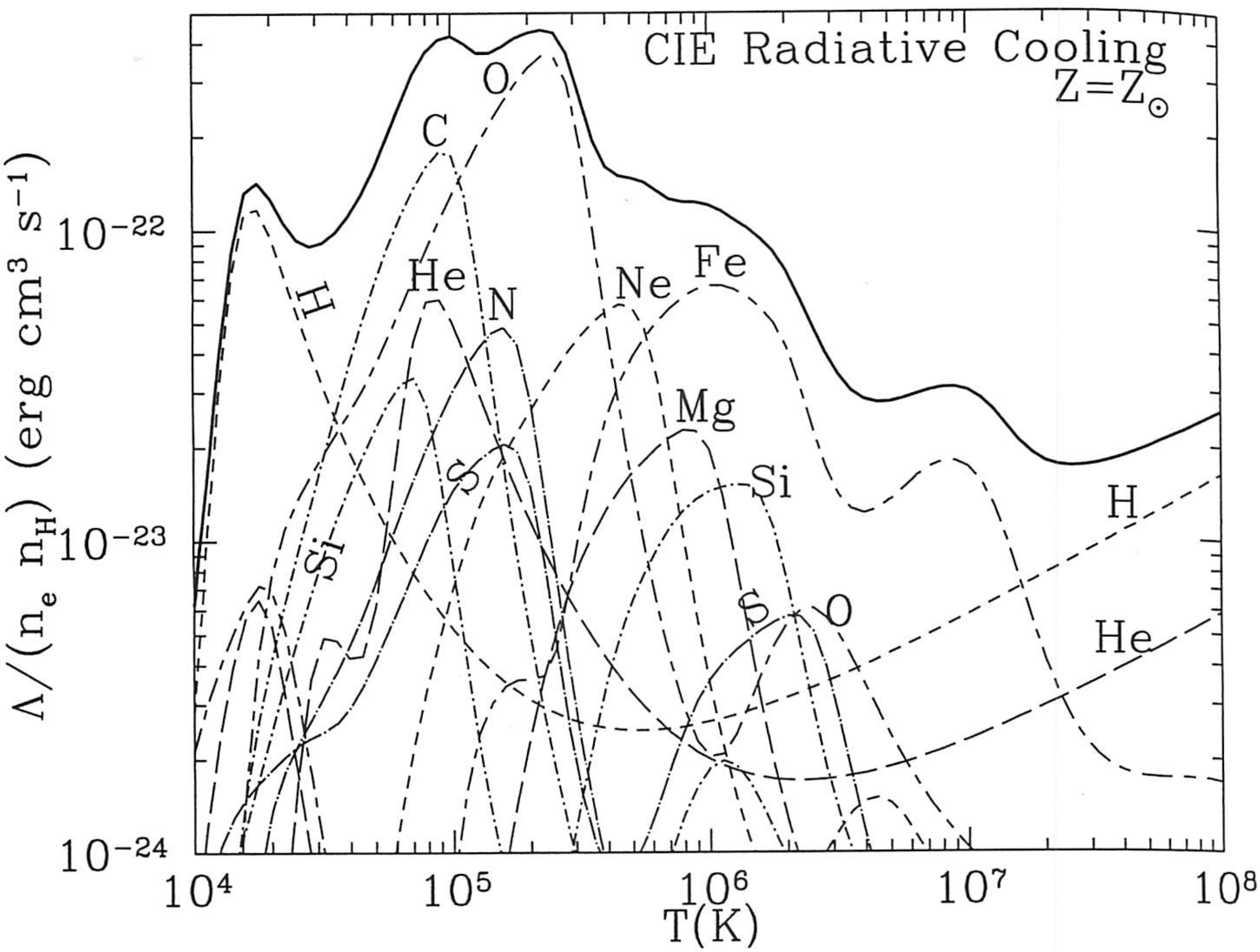

Figure 34.3 Solid line: radiative cooling function $\Lambda/n_e n_H$ from Fig. 34.1, with contributions from selected elements shown.

gas has just been shock-heated, resulting in a sudden increase in the kinetic temperature of the gas, but can also be true when the gas is cooling rapidly, e.g., at $10^{4.9} < T < 10^{5.4}$ K, where the radiative cooling function peaks.

In these cases, the actual radiative cooling rate can be *slower* than CIE (when the gas is cooling faster than it can recombine, so that heavy elements have fewer bound electrons than they would in CIE), or *faster* than CIE (when the gas temperature has been suddenly increased, so that heavy elements are under-ionized). Underionization of elements such as Mg, Si, or Fe can also be an issue when atoms are being sputtered off of dust grains, since they are expected to enter the hot gas as neutral atoms.

1985; Weiland *et al.* 1986) suggests that the MRN grain model should extend to very small grain sizes. The presence of these

the postshock gas; (2) the remnant is expanding into a medium with a lower than average dust-to-gas mass ratio; (3) the dust is

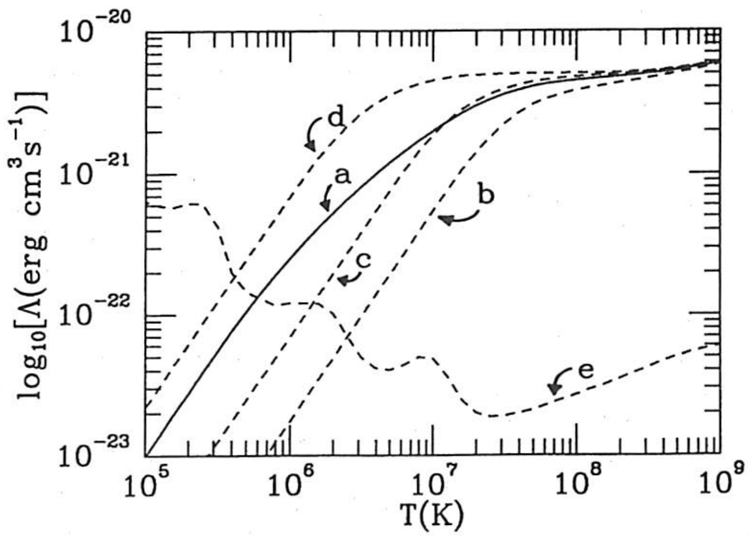

FIG. 4.—The cooling function of the gas via gas-grain collisions, $\Lambda_d(T)$, plotted as a function of gas temperature T, for: the "extended" MRN interstellar dust model (*curve a*); a silicate-graphite mixture of 0.4 μm dust particles (*curve b*); a silicate-graphite mixture of 0.1 μm dust particles (*curve c*); and a silicate-graphite mixture of 0.01 μm dust particles (*curve d*). Curve (*e*) is the cooling function of the gas, $\Lambda(T)$, due to atomic processes (Raymond, Cox, and Smith 1976) and is included in the figure for sake of comparison.

DWEK 1987

New Perspectives on the Interstellar Medium
ASP Conference Series, Vol. 168, 1999
A. R. Taylor, T. L. Landecker, and G. Joncas, eds.

The Eridanus Superbubble in its Multiwavelength Glory

Carl Heiles

Astronomy Department, University of California, Berkeley, CA 94720-3411

L.M. Haffner and R.J. Reynolds

Astronomy Department, University of Wisconsin, Madison, WI 53706

Abstract. The Orion-Eridanus Superbubble is the Rosetta Stone of superbubbles. It is in a middle evolutionary stage, having originated long ago but still being energized by massive stellar winds and supernovae; this means it exhibits the full range of astrophysical processes that occur whenever all of the interstellar gas phases lie in close proximity. It is nearby, so only modest angular resolution is required and, more importantly, it is the only object along the line of sight so its maps can be interpreted unambiguously. We bring together the full range of available data to show that the multiwavelength whole is far more than the sum of its parts. For example, we see the hot interior gas leaking to the outside from a hole in the rear wall of the shell.

1. Overview

The Orion-Eridanus Superbubble (hereafter called the Eridanus Superbubble for brevity) is a big circular structure, the interior of which is filled with XM-band emitting gas and bounded by a wall of denser, cooler gas (see Reynolds and Ogden 1979, Burrows et al 1993, Brown et al 1995). We present various datasets all in a stereographic projection whose pole is centered on the Orion Nebula at $(\ell, b) = (209°, -19°)$. A stereographic projection is an excellent choice for mapping a superbubble in a large region because any small or great circle retains its circular shape, so geometric distortion is relatively small. For example, Figure 1 presents 0.75 keV X-ray data (known as "XM-band emission"). Galactic coordinates are labelled every 30 degrees. The Galactic plane is the nearly horizontal grid line near the top.

1.1. Diffuse X Ray Emission—The Hot Ionized Medium

Figures 1 and 2 map the XM (0.75 keV) and XC (0.25 keV) diffuse X-ray emission (data from Snowden et al 1995b). The XM emission rises rapidly with temperature up to $T \sim 2 \times 10^6$ K; XC emission peaks in a fairly narrow range centered at $T \sim 1 \times 10^6$ K (Snowden et al 1997). The gas need not be at these particular temperatures, but for the sake of convenience we will adopt these temperatures in our discussion. This hot X-ray emitting gas is the Hot Ionized Medium (HIM) of the interstellar medium.

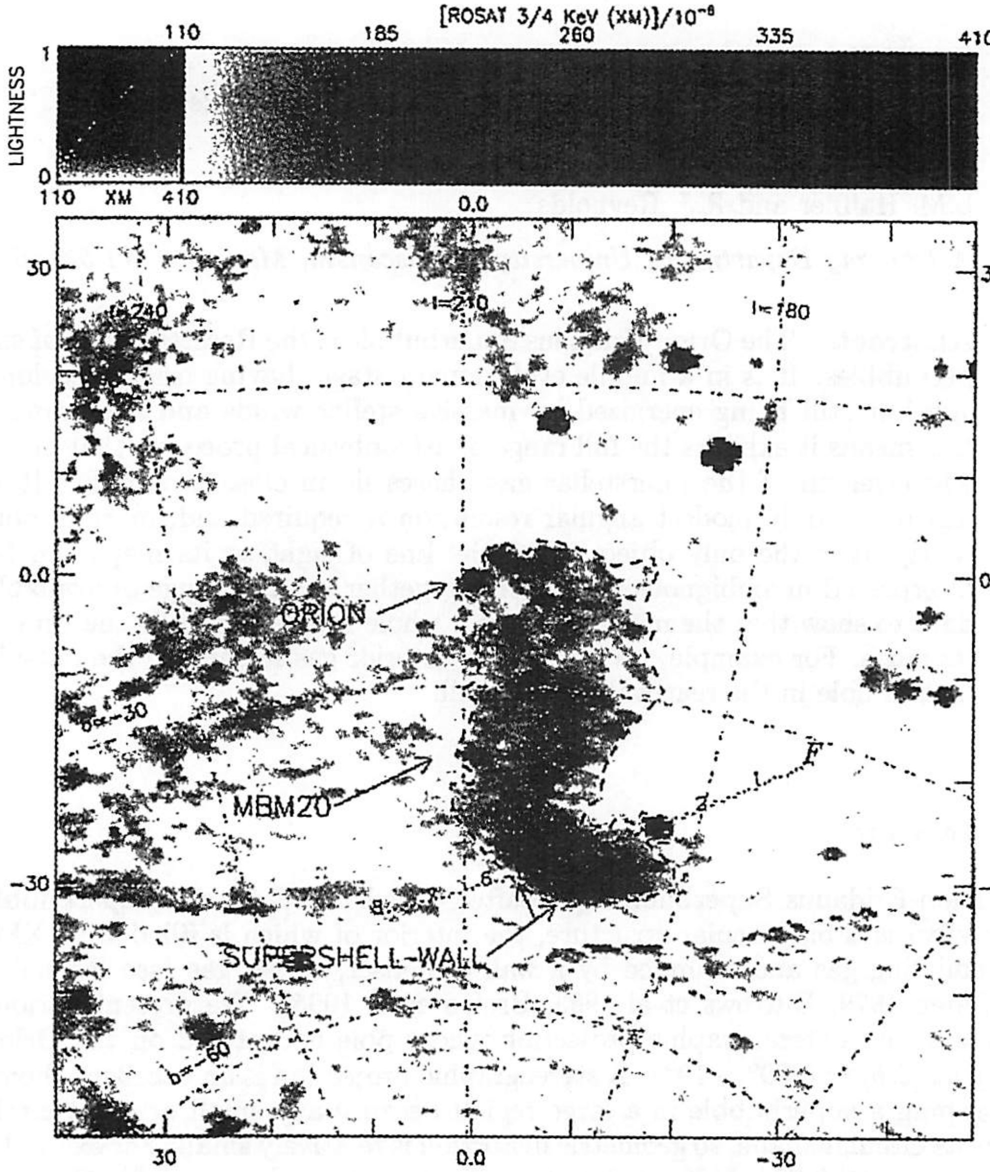

Figure 1. XM-band emission ($\frac{3}{4}$ keV, from gas at $T \sim 2\times10^6$ K) from Snowden et al (1995b). The grey scale is calibrated by the colorbar on top right in units of 10^{-6} ROSAT counts s^{-1} $arcmin^{-2}$; the small square plot on top left shows the same calibration with a graph. Saturated parts of the image exceed the colorbar maximum. Galactic coordinates are labelled on the dashed grid lines. Numbers outside the border refer to angular distance (degrees) from the center of the projection (which is not the center of the image). The heavy dashed line outlines the sharp boundary of the XM emission and the dotted line defines a "slit" for the position-velocity diagrams.

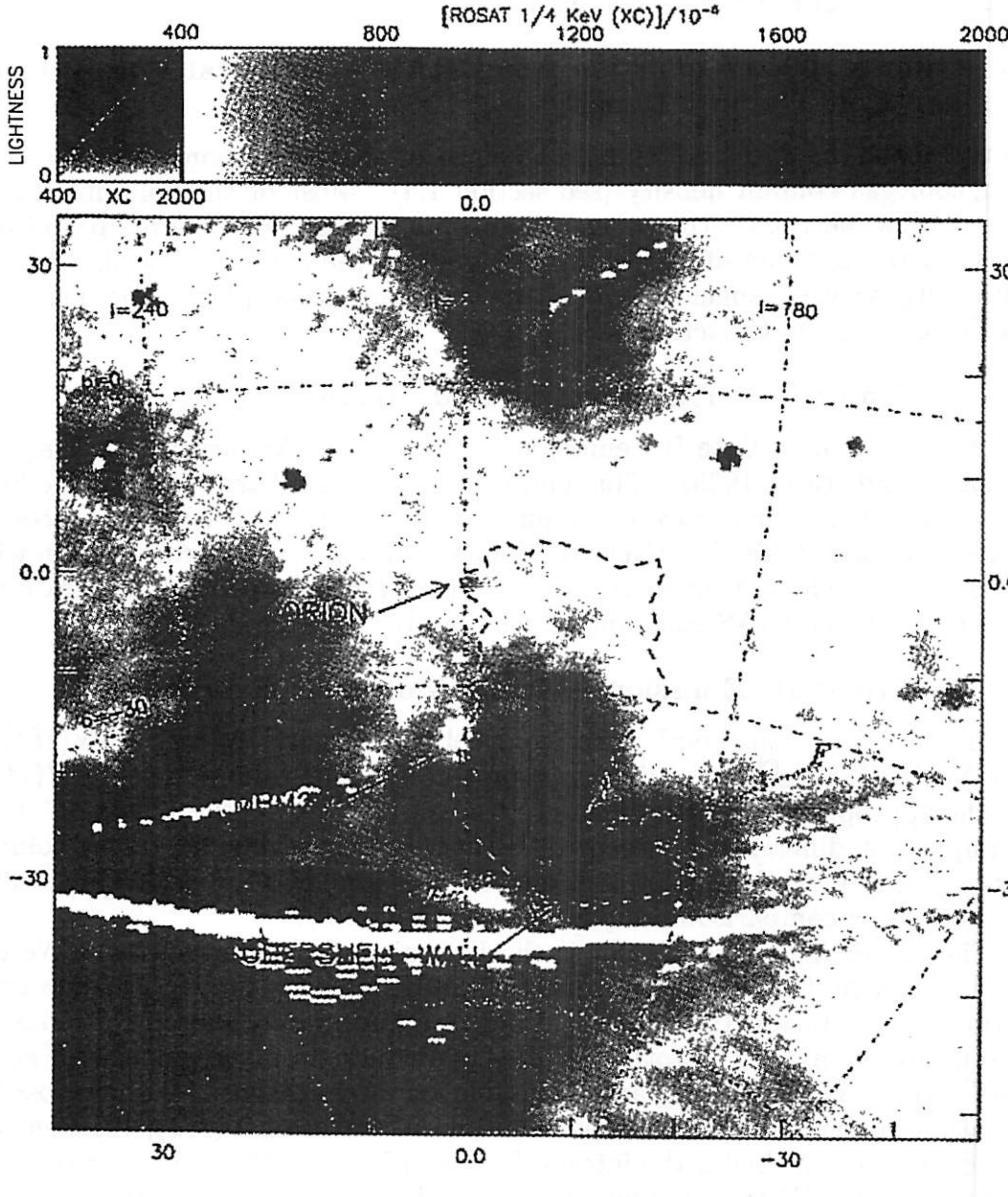

Figure 2. XC-band emission ($\frac{1}{4}$ keV, from gas at $T \sim 1 \times 10^6$ K) from Snowden et al (1995b). See caption for Figure 1.

We annotate a few important features. The XM emission has a sharp boundary, which we trace with a heavy dashed line; in at least some regions this also traces the approximate inner boundary of the supershell wall. The "supershell wall" arrows point to a tangentially-viewed portion of this interface between the HIM and the shell wall gas. This interface bisects the molecular (H_2 and CO) cloud MBM20 (Magnani, Blitz, and Mundy 1985). We also define a "slit" along which we will plot various quantities such as velocity and intensity, as an optical astronomer would place slits on the sky to obtain spectra. Finally, the Orion Nebula is a strong XM emitter.

1.2. Diffuse 100 μm emission from IRAS—The Total Warm, Cool, and Cold Column Density

Figure 3 maps the diffuse 100 μm IRAS emission. This emission traces the total warm/cool gas column density (see section 1.4). Most of the column density is HI ; below we isolate the other components, H_2 and H^+. Three prominent structural components of the warm/cool gas are the supershell wall, which is prominently viewed tangentially near the arrow and other places, the dense gas near Orion, and the Galactic plane.

1.3. Hα Emission—The Warm Ionized Medium

Figure 4 maps the diffuse Hα emission from the WHAM survey (e.g. Haffner, Reynolds, and Tufte 1998). This emission traces the Warm Ionized Medium (WIM), but it does not trace its column density $N(H^+)$. Rather, it traces its emission measure $N(H^+)n_e$. Near the "supershell wall" arrow, comparison with Figure 3 clearly shows that there is an onionskin structure, with the WIM lying inside much of the IRAS emission, which mainly traces HI .

1.4. IR Minus HI Emission—Mainly Molecular Hydrogen

IR emission traces the total warm/cold column density $[N(tot) = N(HI) + N(H_2) + N(H^+)]$ and 21-cm line emission traces the HI column density $N(HI)$; thus the appropriately-scaled difference traces $[N(H_2) + N(H^+)]$. For H^+, note the important difference between its IR and Hα emission: IR traces column density $N(H^+)$, while Hα traces emission measure $EM = N(H^+)n_e$. This means that the comparison provides information on n_e.

The important scaling factor is the IR emission per unit $N(tot)$. We obtained this by performing a least-squares fit of IR intensity to $N(HI)$ (data from Hartmann and Burton 1997) on five different appropriately-chosen Eridanus regions where we expect $N(tot) \approx N(HI)$. We picked only regions with small $N(HI)$. High $N(HI)$ regions are unsuitable for three reasons: (1) their possible saturation of the 21-cm line makes it an invalid tracer of $N(HI)$; (2) their associated extinction shields the interior from starlight, making dust grains cooler and reducing the IR emission per H atom, and (3) their probable associated H_2 provides extra dust unrelated to HI , increasing the IR emission per H atom.

In these fits we did not fit to the 100 μm intensity from IRAS. Rather, we fit to temperature-corrected 100 μm DIRBE data. The DIRBE zero level is better defined than IRAS and the angular resolution is more nearly comparable to the other datasets. Furthermore, the multiwavelength coverage of the DIRBE data allows us to correct for dust temperature; we obtained the correction factor for

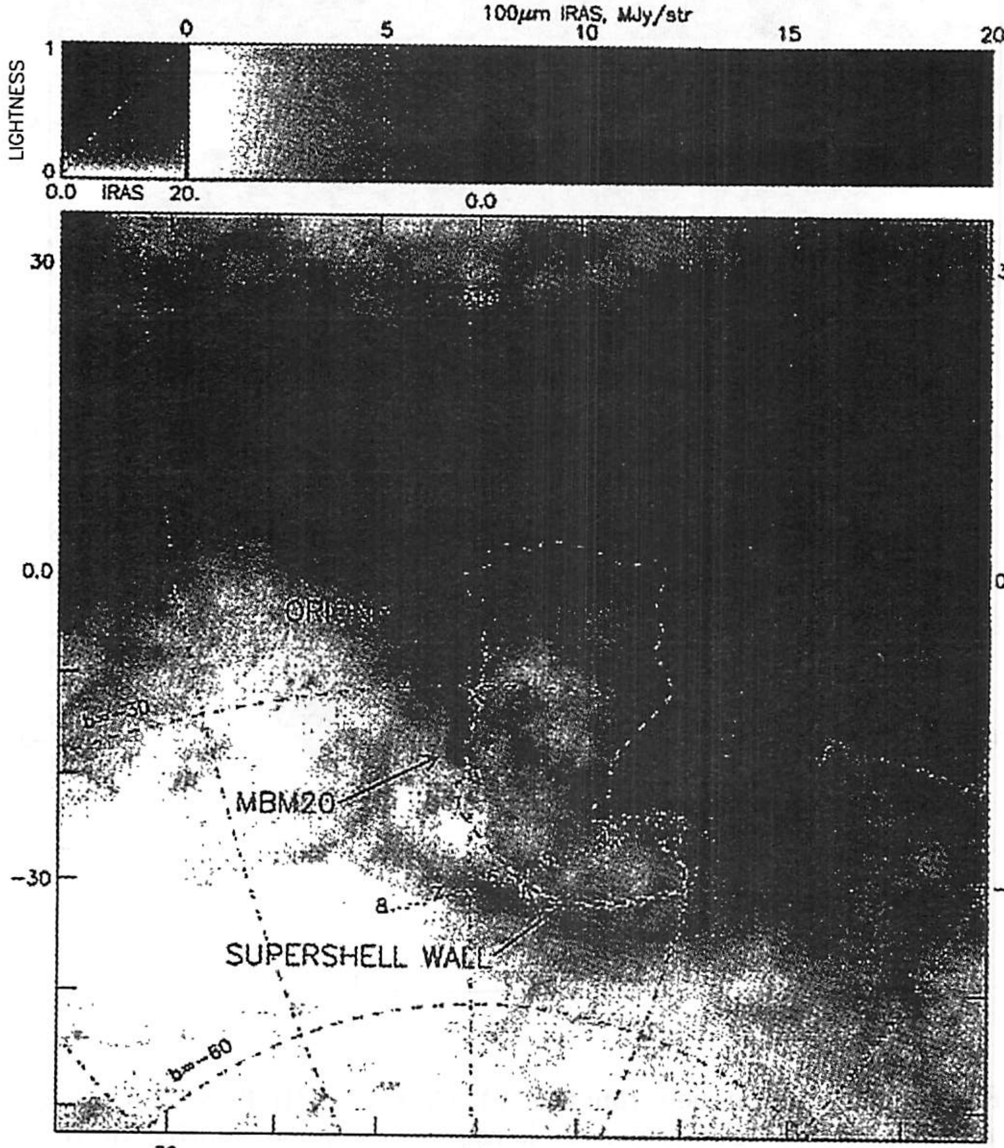

Figure 3. 100 μm emission from IRAS. To obtain $N(HI)_{20}$ in regions of low column density, multiply by about 1.5. See caption for Figure 1.

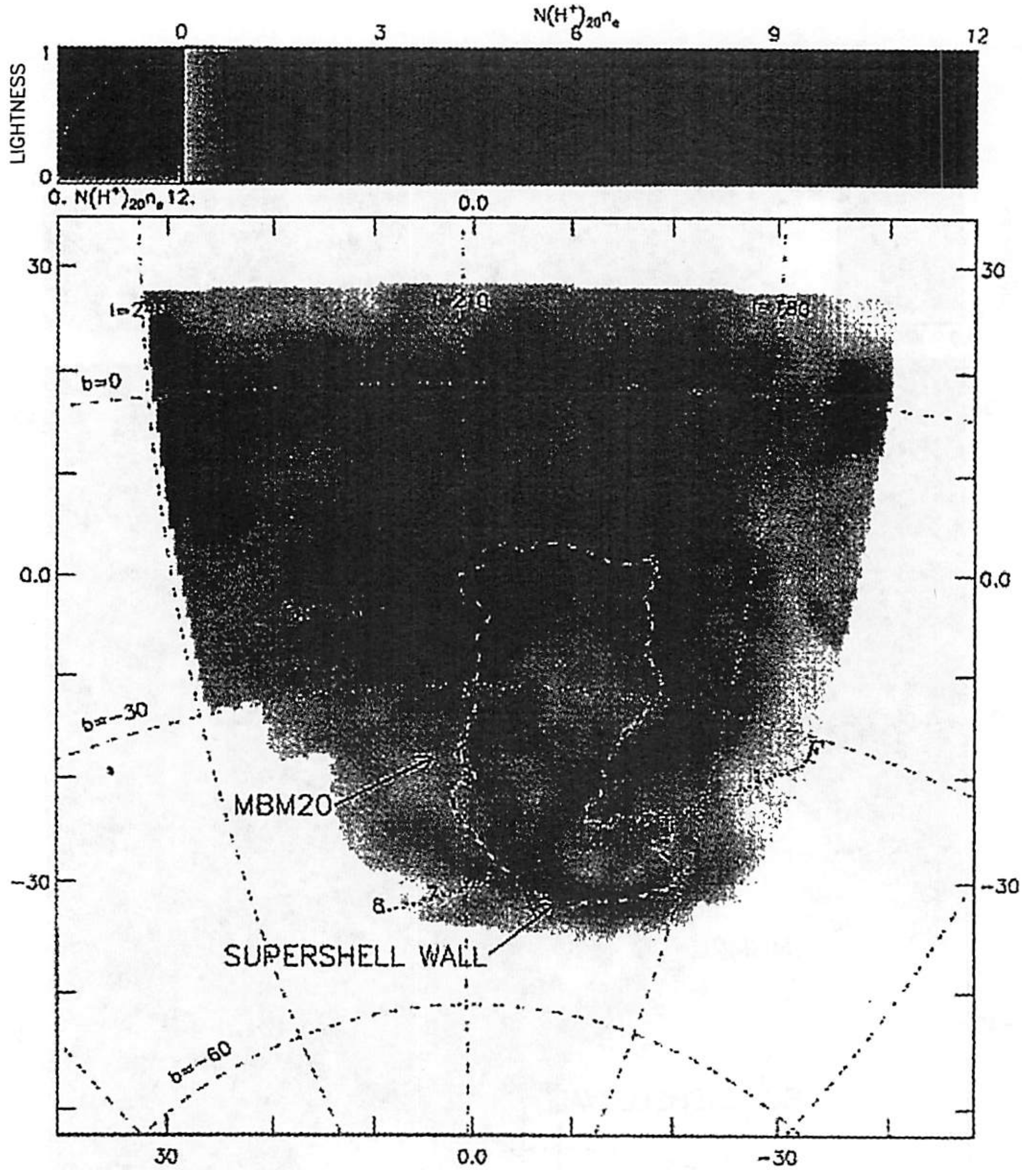

Figure 4. Hα emission from the WHAM survey (Haffner, Reynolds, and Tufte 1998). The grey scale is calibrated by the colorbar on top right and the Hα intensity units are expressed as the emission measure $N(H^+)_{20}n_e$, where $N(H^+)_{20}$ is the ionized gas column density (units 10^{20} cm^{-2}) and n_e the electron volume density (units cm^{-3}); this conversion between Hα intensity and emission measure assumes $T = 10^4$ K and zero extinction. Saturated parts of the image exceed the colorbar maximum. The small square plot on top left shows the same calibration with a graph. See caption for Figure 1.

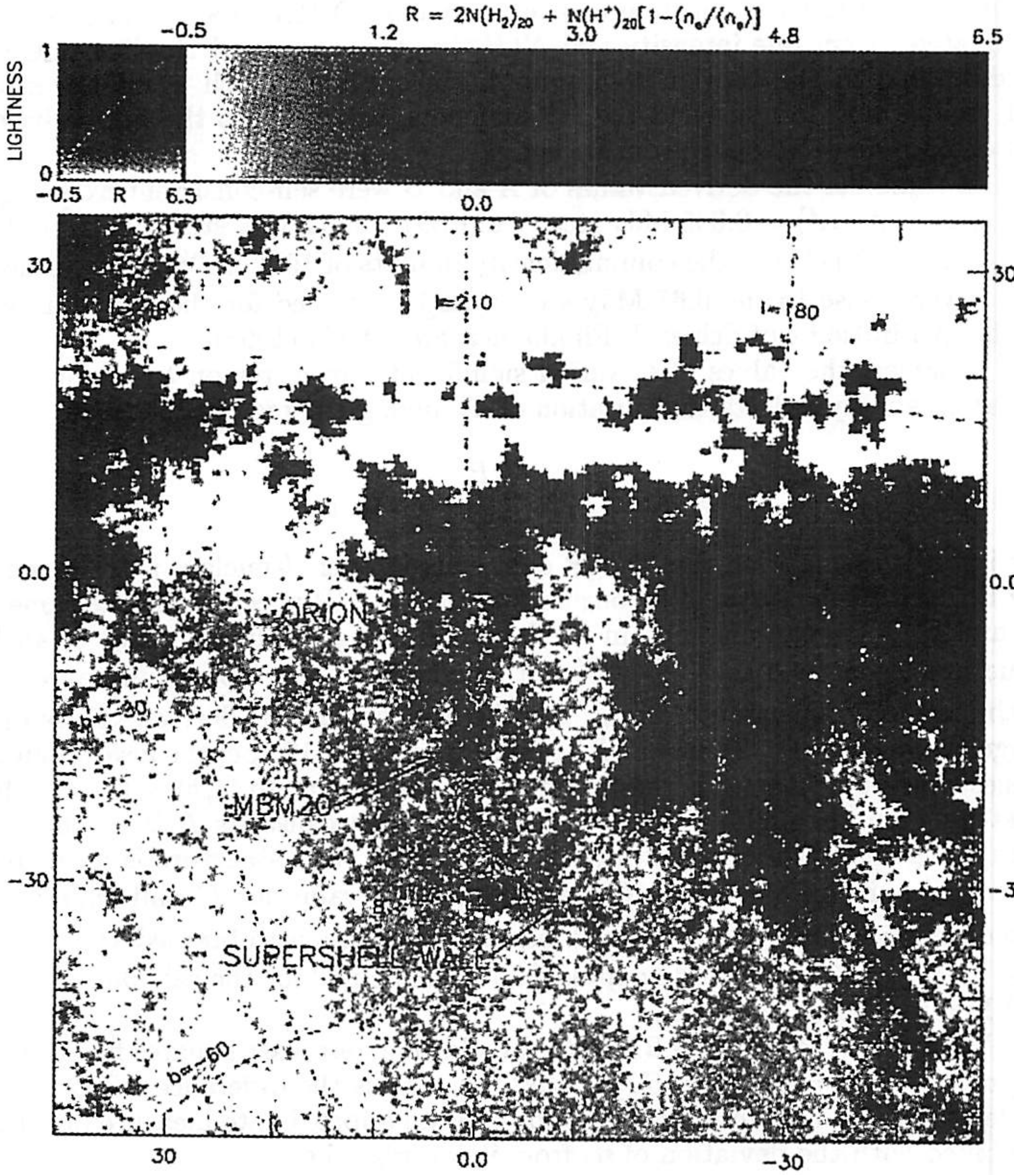

Figure 5. R, the residual temperature-corrected IR emission from equation (3), indicating H_2. The grey scale is calibrated by the colorbar on top right in units of $2N(H_2)_{20}$; the small square plot on top left shows the same calibration with a graph. Saturated parts of the image exceed the colorbar maximum. See caption for Figure 1.

each pixel by a least-squares fit to the 100 μm, 140 μm, and 240μm data. The temperature correction factor scaled the 100 μm intensity to be proportional to the *wavelength-integrated* IR emission.

In each of the five regions we fit the coefficients A, B, and C in the equation

$$IR_{obs} = A + BN(HI) + CN(H^+)n_e\,. \tag{1}$$

Here IR_{obs} is the 100 μm temperature-corrected DIRBE data. $N(HI)$ is the integrated 21-cm line intensity and $N(H^+)n_e$ the integrated Hα line intensity, as described in the caption to Figure 4. In our fits, which avoid the strong HII regions but do not avoid the H^+ filaments, we find that the lion's share of the column density comes from HI not H^+.

In these fits the derived values of A and B were self-consistent from region to region, with $\langle A\rangle = 0.065$ MJy ster^{-1} and $\langle B\rangle = 0.64$ MJy ster^{-1} cm$_{20}^{-2}$ (where cm$_{20}^{-2}$ means $N(HI)_{20}$, the column density in units of 10^{20} cm^{-2}). Our value for $\langle B\rangle$ is very close to the 0.67 MJy ster^{-1} cm$_{20}^{-2}$ obtained for the global average in the quadratic fit of Schlegel, Finkbeiner, and Davis (1998).

However, the values of C varied significantly from region to region. This variation simply reflects the variation of n_e among the regions, because

$$n_e = \frac{B}{C}\,; \tag{2}$$

our implicit assumption that the IR dust emission per H-nucleus is the same for the H^+ and HI is bolstered by our finding that the IR spectrum is the same for HI and H^+. We can also obtain the length L along the line of sight of an H^+ structure, because $L \propto \frac{\text{H}\alpha\ \text{Intensity}}{n_e^2}$, although this is only approximate because of the squared dependence on n_e. For the five regions our derived values of n_e ranged from $0.62 \rightarrow 1.2$ cm^{-3} and L ranged from $32 \rightarrow 120$ pc; the lowest density, longest line-of-sight path is the "filament" running through $(\ell, b) \sim (190^\circ, -40^\circ)$ (just above and roughly parallel to slit F), and because its L is much larger than the plane-of-the-sky width ($\sim 2^\circ$ or ~ 14 pc), this structure is most likely an edge-on-sheet. We define $\langle C\rangle$ as the average value for C and $\langle n_e\rangle = \frac{B}{\langle C\rangle}$ (which means that $\langle n_e\rangle$ is really a harmonic mean); we obtained $\langle C\rangle = 0.84$ MJy ster^{-1} cm$_{20}^{-2}$ cm^{-3} and adopted $\langle n_e\rangle = 0.80$ cm^{-3} for the calculation below and Figure 5.

We expect $IR_{obs} = A + BN(tot)$. In addition, our least-squares fit allows us to predict $IR_{pr} = A + BN(HI) + CN(^+)n_e$. Thus the difference $IR_{obs} - IR_{pr}$ (in least-squares terminology, the residual) is an approximate measure of $N(H_2)$ combined with the deviation of n_e from its average, i.e.

$$R = IR_{obs} - IR_{pr} = B\left[2N(H_2) + N(H^+)\left(1 - \frac{n_e}{\langle n_e\rangle}\right)\right]\,. \tag{3}$$

There is also a minor contribution from saturation of the 21-cm line.

Figure 5 maps this difference, which depends on two terms—the "molecular" and "ionized" terms. The ionized term can be positive or negative: it is negative in regions of large n_e, where a small column density gives bright Hα emission. Thus, dense HII regions would stand out as deficiencies in Figure 5 if they were not associated with molecular clouds. Comparison of Figures 4 and 5 allows one to find regions where ionized gas is absent and the molecular term dominates.

In the Eridanus superbubble we discuss two such regions where H_2 resides. One shows prominently on Figure 5: the CO cloud MBM20. The other is the much less prominent elongated one just above the "supershell wall" label and near Slit F position 6. One might be tempted to disregard the latter's small IR excess as insignificant, but this region is definitely molecular because CO emission has been detected there (Magnani et al 1985). Our detection of these CO clouds by this technique is not necessarily just a tautology because the H_2 angular extents in Figure 5 are large, quite possibly larger than the CO extents (which have not been measured, however).

2. Interpretive Discussion

2.1. The Hot Gas—Not Totally Confined

Looking at Figure 1, we see a sharp, well-defined boundary. At the bottom of the structure, near the "supershell wall" label, is an onionskin structure with XM emission on the inside, an H^+ filament on its bottom edge, and an HI filament outside that. Here we seem to be seeing the superbubble wall edge-on. At the top of the structure, above and to the right of Orion, the XM boundary abuts the H_2 in Figure 5; again, we seem to be seeing the wall edge-on. In fact, the XM-emitting interfaces with dense H_2 over *nearly all* of the top half of the superbubble!

The Barnard Loop, with its half-circular appearance, has intrigued astronomers for a long time. In Figure 4 it is the Hα-emitting top-left half of a full circle. We also find this part of the Barnard Loop to be bright at 408 MHz and to exhibit excess radio emission, far above that emitted from ionized gas alone. In contrast, the bottom-right portion of the full circle exhibits no visible optical or radio emission, as if there were no dense gas for the supernova shock to encounter in this direction. From this direction the XM emission extends into the interior of what would be the full circle of the Barnard Loop. All this is consistent with the idea that the Barnard Loop is a portion of supernova remnant. We can easily imagine the hot gas in the supernova remnant interior expanding, out of this non-dense bottom-right portion, into the interior of the Eridanus superbubble and filling it with the hot gas that emits the XM emission in Figure 1.

Moving down, all the way to the outside of the Eridanus superbubble past the "supershell wall" label, in Figure 2 one sees the XC-band emission extending continuously all the way to the bottom of the image—except for the white parts, which are lunes where there are no data. There are also weak light-grey parts where the XR emission is absorbed by the HI gas, for example the large light grey area just to the left of the two "supershell wall" arrowheads and the left-hand XM boundary line. This is an obvious absorption effect: this area is aligned with the cool gas filaments in Figure 3. This shows that the hot gas lies behind the superbubble wall.

It seems that the XC band emission extends continuously from inside the Eridanus superbubble to the outside, as if the hot gas has leaked across the rear (far side) superbubble wall, presumably through holes in the wall. As it did so it cooled, because there is XC but no XM band emission. Below, in section 2.3, we identify a particular hole where this is happening. There is no reason to assume, as previous authors (e.g. Snowden et al 1995a), that the emission outside of the superbubble wall comes from gas in the "Galactic Halo".

2.2. Evaporation?

Within the superbubble interior there are some bright spots of X-ray emission. We draw attention to two that lie near the molecular regions discussed above: the small XM hot spot on the right hand side of MBM20 (but see cautionary note below), and the large, elongated XM/XC hot spot just above the "supershell wall" arrowhead and below F slit position 4.7. Also, we have bright XM emission from the Orion A HII region, which lies deep inside the superbubble. It seems that there often exist X-ray enhancements near dense regions. These enhancements imply a close physical proximity between the dense regions and hot interior gas.

The XM/XC peaks might be a signature of evaporation, a predicted process for which there are very few observational examples. The basic theory (McKee and Cowie 1977) predicts an enhancement of hot-gas density near an evaporative surface, but not an enhanced temperature; thus the theory does not predict XM peaks in any obvious way.

One cautionary note: Snowden et al (1995a) state that the XM-band enhancements from Orion and MBM20 are only unrelated artifacts (for Orion, the Trapezium stars; for MBM20, the A496 cluster of galaxies). However, the XM band enhancement below F slit position 4.7 certainly comes from the hot gas itself.

2.3. Kinematics on the Lower Right

The kinematics of the Eridanus region is complicated, with both large-scale global aspects and many smaller-scale details. Here we can mention just a few items that we have found. The Barnard Loop is associated with an expanding shell, which strengthens its identification as a supernova remnant. Over much of the left-hand half ($\ell \gtrsim 210°$) of the Eridanus superbubble the HI is at mostly positive velocities and the H^+ at negative velocities, suggesting that the H^+ is confined to the near wall and the HI to the far wall. Over the right hand half the two components are not so simply separated, and there are patches of each on both walls. There are some isolated spots where the velocity structure becomes very complicated.

The kinematics is particularly interesting in one region near the bottom right, inside the almost closed loop formed by the Hα filaments. Slit F passes through the middle of this loop, and Figure 6 exhibits a greyscale image of H^+ in position/velocity space along this slit. In addition to the greyscale, we plot the average velocities of both HI and H^+. The H^+ exhibits a clear expansion signature of the approaching half of a shell. This indicates that this portion of the superbubble wall exhibits a secondary expansion, an expanding minishell within the larger Eridanus superbubble wall.

Although the approaching shell is clear in Hα emission, there is no indication of any HI or H^+ whatsoever in the receding half of this minishell. In this region at least, the hot interior gas of Eridanus is free to escape from the rear of the

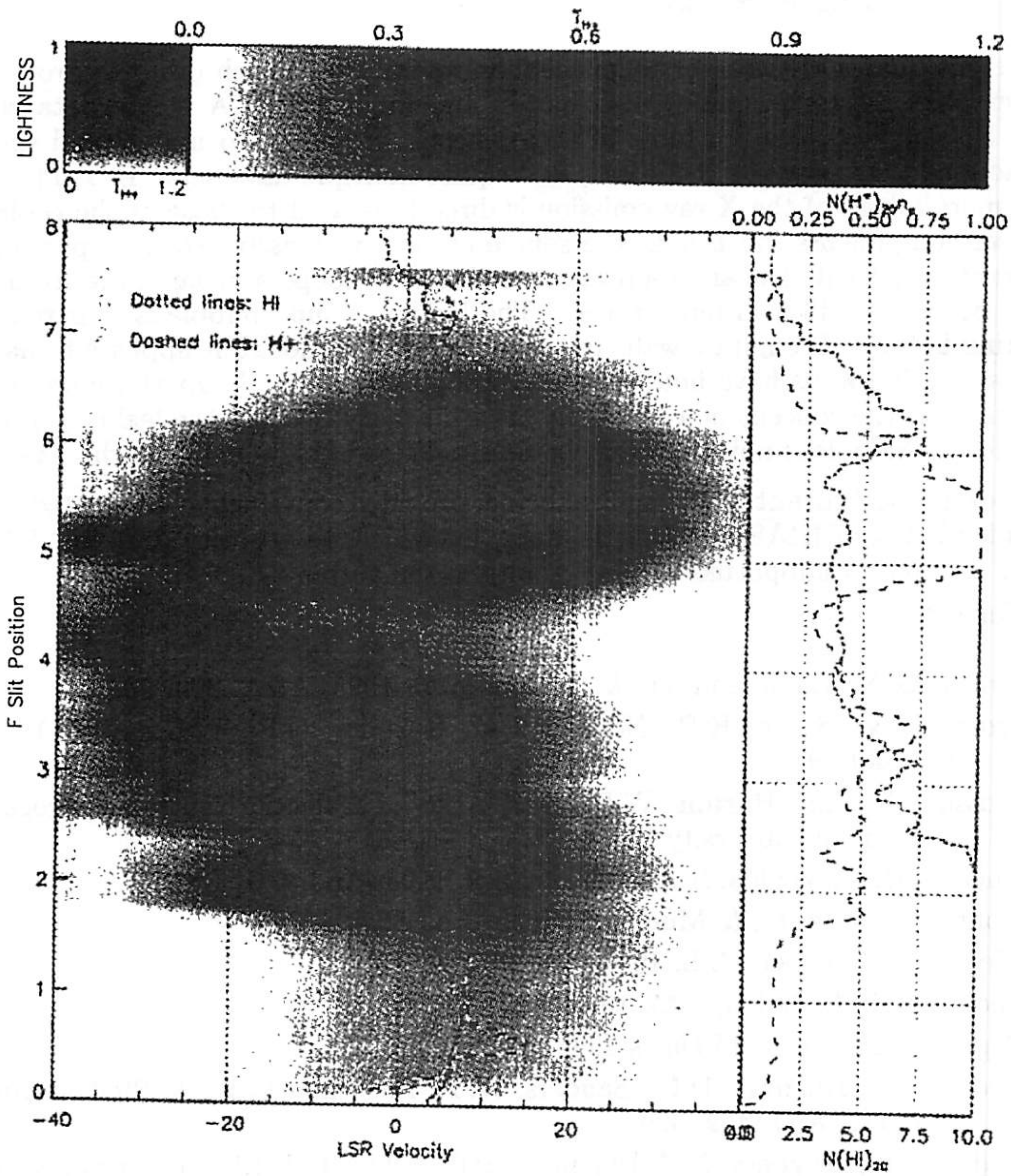

Figure 6. Position-velocity diagram for H^+ along Slit F. The grey scale is calibrated by the colorbar on top right: T_{H+} is the brightness temperature of the 21-cm line in Kelvins that the H^+ *would* radiate *if* it were HI and, also, had $n_e = 1$ cm^{-3} ($T_{H+} \propto n_e^{-1}$); the small square plot on top left shows the same calibration with a graph. Saturated parts of the image exceed the colorbar maximum. The dotted and dashed lines on the image show the mean velocity of HI and H^+, and the graphs on the right show the column density of HI and the emission measure of H^+.

superbubble to the outside. This must be one of the "holes in the superbubble wall" to which we referred above in section 2.1, where we argued that the XC-emitting gas has escaped from the interior through holes in the wall.

3. Concluding Remarks

Different phases of the interstellar medium interact with each other to produce observable effects in spatial distribution and kinematics. A single data set, e.g. HI , allows us to see some of these effects. However, to understand the i teractions that produce the effects we require multiple data sets. In Eridanus the morphology of the X-ray emission is directly related to those of the cooler, denser components, both near the source of energy (massive stars of previous generations, located near Orion and the Barnard Loop) and far away from it (the bottom portion in our figures). The Eridanus superbubble is apparently leaking hot gas through its walls to the outside, even though it appears to have a "cap". The walls have holes. This is probably true of all superbubbles, and means that the concept of a "chimney" is a bit fuzzy because the leaking of hot gas to the halo does not require a classically-defined "blowout" into the halo.

Acknowledgments. Doug Finkbeiner provided conveniently formatted and gridded maps of IRAS and DIRBE data, for which we are very grateful. This work was partly supported by NSF grants to the authors.

References

Brown, A.G.A., Hartmann, D., & Burton, W.B. 1995, A&A, 300, 903.

Burrows, D.N., Singh, K.P., Nousek, J.A., Garmire, G.P., & Good, J. 1993, ApJ, 406, 97.

Hartmann, D., and Burton, W.B. 1997, Atlas of Galactic Neutral Hydrogen, Cambridge University Press.

Haffner, L.M., Reynolds, R.J., & Tufte, S.L. 1998, ApJ, 501, L83.

Magnani, L., Blitz, L., & Mundy, L. 1985, ApJ, 295, 402.

McKee, C.F., & Cowie, L.L. 1977, ApJ, 215, 213.

Reynolds, R.J. & Ogden, P.M. 1979, ApJ, 229, 942.

Schlegel, Finkbeiner, and Davis 1998, ApJ, 500, 525.

Snowden, S.L., Burrows, D.N., Sanders, W.T., Aschenbach, B., & Pfeffermann, E. 1995a, ApJ, 439, 399.

Snowden, S.L., Freyberg, M.J, Plucinsky, P.P., Schmitt, J.H.M.M., Trümper, J., Voges, W., Edga, R.J., McCammon, D., & Sanders, W.T. 1995b, ApJ, 454, 643.

Snowden, S.L., Egger, F., Freyberg, M.J, McCammon, D., Plucinsky, P.P., Sanders, W.T., Schmitt, J.H.M.M., Trümper, J., & Voges, W. 1997, ApJ, 485, 125.